On the role of meridional winds in a coupled model of ENSO

by

Claire Périgaud (*), Stephen E. Zebiak (**), Frédéric Mélin (*),
Jean-Philippe Boulanger (*) and Boris Dewitte (*)

submitted to Journal of Climate, February 14, 1996

Addresses:

(*) Jet Propulsion Laboratory, MS 300/323, 4800 Oak Grove Drive, Pasadena, CA 91109, USA. email: cp@pacific.jpl.nasa.gov

(**) Lament Doherty Earth Observatory, Palisades, NY 10964, USA.

Abstract

The role of the interannual meridional wind anomalies in a simple coupled tropical Pacific ocean-atmosphere model is investigated. It is found that these anomalies play a key role in maintaining finite amplitude interannual variability in the coupled simulations. When the meridional wind stress anomalies are not allowed to feed back to the ocean, the simulated ENSO oscillations are damped out within a few years. This happens irrespective of initial conditions.

During a warm (cold) event, the simulated meridional wind stress anomalies drive covergent (divergent) surface currents in the equatorial east Pacific, inducing downwelling (upwelling) anomalies that act to strongly reinforce the SST and wind anomalies. This is in contrast to the model zonal wind stress anomalies, which due to the tendency to reverse sign in the eastern Pacific, induce upwelling (downwelling) anomalies in the east, and SST patterns with weaker net positive feedback.

Observed wind stress anomalies are also analyzed, and found similar in certain respects to those of the coupled model in the near-equatorial region. The dominant observed wind stress pattern shows a reversal of the zonal component between the central and far eastern Pacific. The east Pacific meridional stress anomalies imply a vertical current of opposite sign, and similar magnitude to that induced by the zonal stress, These features, consistent with the model results, suggest the importance of meridional wind stress anomalies in the real climate system.

1. Introduction

More than twenty years ago, Bjerknes (1969) postulated that the El Niño Southern Oscillation (ENSO) could be explained as a self-sustained

cycle based on the coupling between the sea surface temperature (SST) and the trade winds. Later, the theory of linear equatorial ocean dynamics (e.g. Moore and Philander, 1977; Cane and Sarachik, 1976) provided clues for the understanding of ENSO, and contributed to the current paradigm for ENSO variability, commonly referred to as the delayed oscillator (Schopf and Suarez, 1988), involving equatorial long waves generated by zonal winds, their propagation and reflection at the boundaries, and to a lesser extent, their role in advecting the heat across the basin (Battisti, 1988),

Most of the simple coupled models used to simulate ENSO (e.g. Zebiak and Cane, 1987; Battisti, 1988; Kleeman et al, 1995) are based on the assumptions of a shallow-water ocean model. Forced by winds, such models respond in terms of Kelvin and Rossby waves (Cane and Sarachick, 1979; Busalacchi and O'Brien, 1981). Several authors have found evidence of equatorial waves in reality, using sea level from in situ data (e.g. Knox and Halpern, 1982; Kessler and McPhaden (1 995) or from satellite data (e.g. Miller et al, 1988; Delcroix et al, 1994; Boulanger and Menkes, 1995).

Although equatorial long waves account for a large part of the ocean dynamic variance (in models or data), they may not be sufficient to explain the observed ENSO variability. Jin and Neelin (1993) have introduced the concept of SST modes and ocean dynamics modes which give to the coupled system a variety of oscillatory regimes involving different physical mechanisms. In all previous studies, little attention has been paid to the role of the meridional wind in ENSO. Indeed the delayed oscillator theory does not give any role to the meridional wind. Meridional wind stress anomalies do not generate Kelvin waves. Most of the conceptual or modeling approaches used for ENSO (e.g. Lau 1981; McCreary and Anderson, 1984; Graham and White, 1988; Battisti, 1988; Schopf and Suarez, 1988: Cane et

al, 1990; Neelin, 1990) assume that the meridional wind stress component is zero. Although some authors have sought solutions to the complete system (Hirst, 1985; Yamagata, 1985, Cane and Zebiak, 1985; Battisti and Hirst, 1989), the oscillatory behaviour of their models was explained in terms of zonal wind stress anomalies only. Although not particularly focusing on the role of the meridional wind, Philander and Hurlin (1988) and Barnett et al (1 991) do consider the meridional structure of the ENSO physics. These authors found an important role of the meridional advection in the heat budget of the eastern basin, Recently, Xie (1994) examined the role of the climatological meridional wind in maintaining the equatorial asymmetric ITCZ. In the present paper, we examine the question of the role of meridional wind anomalies in ENSO in the context of the simple coupled ocean-atmosphere model of Zebiak and Cane (1987; hereafter, ZC). In the following, we will use the abbreviations MWSA and ZWSA for meridional wind stress anomalies and zonal wind stress anomalies, respectively.

This paper is organized as follows. In section 2, we present results showing the importance of MWSA to the simulated interannual variability. Section 3 addresses the question of which components of the model physics are significantly affected by the MWSA. In section 4, we analyze the eastern equatorial Pacific heat budget in detail. The impact of the observed MWSA in an ocean-only forced calculation is presented in section 5. In section 6, we make some direct comparisons between simulated and observed wind fields, and analyze their impacts on upwelling and SST evolution, A summary, and some discussion of the results are provided in section 7.

2. **Impact of MWSA on the simulated ENSO variability**

We present first the results of an experiment without any anomalous meridional forcing; that is, the MWSA is artificially set to zero at each time step within the ocean model update (experiment CPD.TY0). It is compared to the results simulated in the standard case (experiment CPD.STD), where both wind stress components are taken into account, The index used to examine the oscillations of the model in this paper is the Nino3 SST index, i.e. the SST anomalies averaged over the region (5°S-5°N, 150°W-90°W). The index is plotted over a fifteen year period in Figure 1a for bet} experiments. Whereas the index simulated in experiment CPD.STD oscillates with a 3 to 5 year-period as expected, the one simulated in experiment CPD.TY0 remains close to zero over the whole period. This suggests that the MWSA are crucial for the ZC model to simulate ENSO-like oscillations.

Various initial conditions (weak or strong anomalous states at different seasons) were tested to examine the robustness of this result. The experiments presented in Figure 1 a were initialized with the conditions of January 1980 provided by the model run in a forced mode with FSU winds, as described by Cane et al. (1986). The January 1980 conditions correspond neither to an El Niño nor a La Niña situation; all the fields are characterized by weak anomalies. We tested various cases which contrast with this situation. The index simulated by the model initialized during a very strong El Niño situation (January 1983) is presented in Figure lb for both experiments. For a period of a year or so, the index simulated by CPD.TY0 is similar to the one simulated by CPD.STD. Thereafter, it shows very weak oscillations, Experiments using initial conditions from April, July, and October verified that the conclusion does not depend on season (not shown). Other experiments were initialized from an initial external wind perturbation

in the western Pacific, as in Zebiak and Cane (1987). The Niño3 index from an extreme case among these experiments - one in which oscillations are maintained for two ENSO cycles - is presented in Figure 1 c. In the long term even this run decays to the zero anomaly state. In fact, it is clear from this experiment that the neglect of MWSA switches the stability of the model's zero anomaly state from unstable to stable,

In an additional experiment, we put the meridional wind anomaly, instead of the MWSA, to zero. This is not the same experiment as CPD.TY0, as the wind stress anomaly is computed from the anomalous and the prescribed climatological wind components using a standard quadratic bulk formula. This experiment gives a similar result: finite amplitude variability can be sustained only for a few years.

The unambiguous conclusion is that the anomalous meridional wind (or wind stress) is necessary to sustain the interannual variability of the coupled model.

3. **Characteristics of MWSA impact**

The ZC ocean model has two components, representing the baroclinic dynamics (shallow water equations; see Eq. A4 to A6 in ZC) and the surface layer, where the Ekman shear currents are computed (Eq. A8 to Al 1 in ZC). The wind stress anomaly is an input for these two model components. In experiment CPD.TY0, the meridional wind stress anomaly was put to zero in both.

In order to determine how the MWSA play a significant role in the ZC model, it was first put to zero in the baroclinic model only and not in the surface layer model (experiment CPD.TYb). This gives results in very close agreement with run CPD.STD (Figure 2a), The complementary experiment

was also done: the baroclinic model was forced with the full wind, and the MWSA was put to zero only in the surface layer equations. In this case, the Niño3 index remains close to zero, similar to run CPD.TY0 (Figure 2a). Therefore, the interannual MWSA play a major role in the ENSO-like oscillations simulated by the ZC model through the generation of Ekman currents, The impact on the baroclinic ocean dynamics is not crucial. The latter point is in agreement with all the theoretical studies of ENS() based on the baroclinic dynamics only. Since these theories do not consider the surface layer dynamics explicitly, no role whatsoever has been assigned to the meridional wind stress - in contrast with the present results.

Additional experiments were run in order to identify in which regions of the tropical Pacific the MWSA play a key role. The variance of the simulated MWSA is maximum off the equator, at 15°N-140°W and at 12°S-120°W. Nevertheless, as proposed by Battisti (1 988), the off-equatorial winds may not play a role in the coupled oscillations. We ran the model with the MWSA forcing the surface layer filtered at each time step as in Battisti (1988): the MWSA are multiplied by a function which is equal to 1 between 5°S and 5°N, zero beyond 9° of latitude and linearly decreasing between 5° and 9° of latitude (experiment CPD.TYEk.filtoff). The experiment gives results very C1OSC to the standard run (Figure 2b). In another experiment (CPD.TYEk.filteq), the MWSA were filtered in exactly the opposite manner. This run does not sustain interannual oscillations (Figure 2b). Thus, it is in the equatorial band (5°S-5°N) that the MWSA play a crucial role. Although the anomalies are not especially strong there, their impact is enhanced by the strong atmosphere-ocean coupling of this region.

4. Analysis of the MWSA role in the model heat budget

In the equatorial band, the variance of the simulated MWSA is found maximum in the eastern Pacific, over the Niño3 region. In this section, we examine how the MWSA can indeed affect the SST variations in the eastern equatorial Pacific, The various terms involved in the simulated SST variations are:

the local rate of SST changes in time:

$$\partial T / \partial t \qquad (1)$$

the zonal advection:

$$-U.(\overline{T} + T)_x \qquad (2)$$

$$-\overline{U}.TX \qquad (3)$$

the meridional advection:

$$-V.(\overline{T} + T')_y \qquad (4)$$

$$-\overline{V}.T_y \qquad (5)$$

the vertical advection:

$$-\{M(\overline{w}_s + w_s) - M(\overline{w}_s)\}.\overline{T}_z \qquad (6)$$

$$-M(\overline{w}_s + w_s).(T - T')/H_1 \qquad (7)$$

and the damping:

$$-\alpha_s.T \qquad (8)$$

T is the sea surface temperature anomaly, U and V are the zonal and meridional surface current anomalies, $\overline{U}$ and $\overline{V}$ are the prescribed zonal and meridional climatological surface currents, w_s and $\overline{w}_s$ are the anomalous and mean vertical currents at the base of the mixed layer . M(x) is the function equal to x if x is positive, and equal to zero if x is negative, T_e is the temperature of entrained water, H_1 is the depth of the mixed layer, $\overline{T}_z$ is the prescribed mean vertical temperature gradient. The reader can refer to

the Appendix in ZC where all the functions and parameters are described, The surface current anomalies U and V are computed from the baroclinic current anomalies and the Ekman shear induced by the wind anomalies. The vertical current anomalies w_s are estimated from the divergence of surface current anomalies, assuming the surface layer has fixed depth,

Each of these terms simulated by CPD.STD was averaged over the Niño3 region and plotted as a function of time (Figure 3). As noted by several authors (e.g. Philander and Seigel, 1985; Battisti, 1988; Barnett et al, 199 1), several terms contribute to the SST tendency, The terms which involve the MWSA are (2), (4), (6) and (7), Among them, term (4) has the weakest amplitude and term (6) the strongest, but most importantly, term (6) is the one which has the strongest anticorrelation with the damping term (8). Term (6) leads term (8) by about two months, Term (6), which represents the anomalous upwelling of prescribed mean temperature gradient, has a positive feedback on growing anomalies.

The terms in the SST equation are nonlinearly dependent on the MWSA in the full coupled run, and individual effects are not strictly additive. Thus, various experiments were run to test the role of the MWSA on individual terms. From these, wc determined that it is indeed the sensitivity of term (6) which accounts for the behavior without the MWSA previously described.

Thus, the MWSA induce convergent (divergent) surface currents near the equator during a warm (cool) event, forcing a downwelling (upwelling) that enhances the warming (cooling) tendency. This positive feedback contributes substantially to the maintenance of finite amplitude oscillations in the coupled system,

Term(6) is analyzed below in more details for run CPD.STD. The near-equatorial vertical current anomaly (the total one due to the divergence of the baroclinic currents and that of the Ekman currents) is presented in Figure 4a for the height of a typical warm event, The anomaly corresponds to a strong downwelling over most of the central and eastern equatorial Pacific, and upwelling near the eastern boundary, Most of the total anomaly is due to the component derived from the Ekman shear induced by the ZWSA as shown on the equatorial section (compare the dashed and the thin solid lines in Figure 4b). This latter component is almost proportional to the ZWSA (compare the thin and thick solid lines in Figure 4b). The downwelling is maximum at 130°W, and decreases sharply toward the east. Indeed the vertical current anomaly is an upwelling east of 95°W and winds are easterlies there. Along the equatorial section, the vertical anomalous current due to the MWSA (thin solid line in Figure 4c) is a downwelling in the central and eastern Pacific, It is weak in the central Pacific, but its amplitude is maximum in the eastern Pacific. This component is almost entirely explained by the meridional derivative of the MWSA (thick solid line in Figure 4c). Because the prescribed mean vertical gradient of temperature is stronger in the eastern Pacific than in the central Pacific, the SST changes induced by the vertical current anomalies are the largest in the eastern Pacific (Figure 4d). The prescribed gradient has a strong local minimum at 164°W, which explains that the SST warming induced by the ZWSA presents a sharp increase east of this point up to 125°W. In the far eastern equatorial Pacific, the MWSA have a warming impact and the ZWSA have a cooling one, The opposite picture is found for cold events.

Thus, the upwelling (downwelling) anomaly related to the ZWSA alone tends to reverse the large-scale warming (cooling) tendency in the far

eastern basin, and the resulting SST gradients can enhance the easterly (westerly) winds in this region during a developing warm (cold) event, The result in a coupled run is that the integrated wind forcing is much reduced, and events can terminate abruptly (from the east). The coupled effect is actually large enough to eliminate the large-scale coupled instability. On the other hand, when the MWSA are included, the vertical current anomaly is enhanced in the eastern Pacific in the direction of that of the central Pacific anomaly. In the presence of a sharply eastward-increasing mean vertical temperature gradient, this creates SST anomalies that are more zonally uniform, or even increasing eastward, leading to a much reduced eastern wind reversal, a larger integrated wind forcing, and a stronger coupled instability.

In summary, the results have highlighted two processes in the eastern equatorial Pacific. Taking the case of a warm event, the model simulates a ZWSA which induces an upwelling anomaly - a negative feedback tendency. At the same time, the model simulates MWSA which induce a downwelling anomaly - a positive feedback tendency. Both developments are highly confined to the eastern Pacific. Their importance in this coupled model is amply demonstrated, but is there any evidence of counterparts in reality? It is to this issue that we turn next,

5. **Role of the MWSA in the ocean model forced by observed winds**

The ZC ocean model component was run in an "uncoupled" mode, forced by prescribed wind stress anomalies. The ZC ocean model, starting from rest, was forced by the FSU wind stress anomalies from January 1964 to April 1995 (experiment CR. STD). Starting from the conditions in January

1980, we ran an experiment (CR.TY0) which consists of forcing the ocean model with only the zonal wind stress anomalies (the MWSA being artificially set to zero), The Niño3 indices simulated by the two experiments are very similar, with maximum differences (occurring in July 1983) less than 0.5°C (Figure 5a).

The magnitude of the signal due to the MWSA in a forced context is thus small, relative to the one due to the ZWSA. This does not mean that the meridional wind has a negligible contribution in a coupled context or in reality, however. What matters at least as much as the amplitude is the spatial pattern of the SST anomaly associated with the meridional wind stress. We computed the SST differences between the two simulations over 1980-1995. These fields often show a strong north-south gradient near the equator. As an example, the SST anomalies simulated by the two experiments and their difference for January 1983 are shown in Figure 5b-5d. It is seen that in the central Pacific, the MWSA are responsible for a warming tendency south of the equator and a cooling tendency north of the equator. East of 120°W, the MWSA induce a warming tendency near the equator and a cooling tendency further poleward.

Thus the MWSA are responsible for SST changes which have a spatial pattern somewhat different from the ones induced by the ZWSA. If they were similar, then it would be possible to recover the full model behavior with only the ZWSA forcing, but slightly altered coupling parameters. This is not the situation. In any case, it is clear that the SST anomalies induced by the MWSA will in general force both meridional AND zonal wind anomalies, and these feedbacks in principle can lead to much larger signals. Accordingly, one cannot at this stage rule out the possibility of a significant contribution of the MWSA to the observed climate variability.

6. **Comparison between observed and simulated wind stress anomalies**

Wind stress anomalies from observations (FSU analyses) and from the CPD.STD run were compared by decomposing each into EOF's over the model domain, A period of 23 years was used for each decomposition; for the observational data, the period corresponds to the years 1970-1992. The first EOF explains 78% of the variance. for the simulated fields, 14% for the observed fields. The amplitude maps of the first EOF are presented in Figure 6 (with amplitudes normalized to have the same variance on average over the region 5°S - 5°N).

The observed and simulated ZWSA in the equatorial band agree to some extent. As expected, they have a maximum in the central Pacific, The primary discrepancies are that the simulated maximum is located to the east of the observed one, and the zonal gradient along the equator is much stronger for the simulations than for observations east of 120°W. Nevertheless, as for the simulated winds, the observed zonal wind patterns exhibit a reversal in the eastern equatorial Pacific during ENSO extremes.

The observed and simulated MWSA patterns agree in being of similar overall amplitude (relative to the amplitude of the zonal anomaly). Both show coherent anomalies in the northern tropics, but with the simulated wind maximum located considerably northeast of the observed one. In the south, the observed winds are coherent in the central and western basin only. The simulated wind pattern is more coherent, with strongest signal displaced considerably to the east of that from observations.

The upwelling anomalies induced by each component via the Ekman shear were also computed for the observed and model stress EOF. The current anomaly induced by the observed winds present some similarities

with the simulated one, although the strong downwelling in the central Pacific is located to the west of the simulated one (compare Figure 7a with Figure 4a), This is primarily due to the offset to the east of the simulated ZWSA. Besides this major discrepancy, the signs of the current anomalies induced by either wind component and their relative amplitudes are in good qualitative agreement in the equatorial Pacific east of 120°W. There, for both observed and model fields, it is found that the current anomaly is weaker than the one induced by the ZWSA in the central Pacific, the ZWSA induce an upwelling (Figure 7b) and the MWSA induce a downwelling (Figure 7c). The agreement is even clearer when considering the SST changes induced by the wind anomalies (Figure 7d). For observations and model, the ZWSA has a cooling impact and the MWSA has a warming impact in the eastern equatorial Pacific.

The observations hint of the same near-equatorial positive and negative feedbacks associated with MWSA and ZWSA as shown by the model. Conclusions must be tentative, however, because of the notable differences between observed and modeled fields, and because of the much more limited variance contained in the. observed versus the simulated EOF fields.

7. **Summary and Discussion**

In this paper, we have examined the role of the meridional wind component in ENSO, a question which has previously been neglected. The results are based on simulations with the ZC model. The MWSA are found to play a key role in sustaining the ENSO-related variability of this coupled model. This key role is played via the vertical current anomaly induced by the Ekman divergence in the equatorial eastern Pacific. In agreement with

Barnett et al (1991) and Jin and Neelin (1 993), these results highlight the importance of the Ekman forcing in the heat budget of the tropical Pacific.

During a growing warm (cold) event, the meridional wind drives convergent (divergent) surface currents which induce an equatorial downwelling (upwelling) anomaly in the far eastern Pacific, Without this positive feedback, the coupled model cannot sustain interannual variability, because the reversal of the zonal wind stress simulated by the model at the eastern boundary prevents the SST anomalies from growing, and reduces the large-scale atmosphere-ocean coupling. The key patterns of the wind responsible for such coupled feedbacks are the ZWSA being easterlies (westerlies) and the MWSA being convergent (divergent) in the equatorial Pacific east of120"W.

The first EOF of the observed winds also contain these patterns, Comparison between simulated and observed winds suggests that the model's wind reversal may be unrealistically strong. This deficiency of the ZC model has been examined in several papers (Zebiak, 1986; Zebiak, 1990; Perigaud and Dewitte, 1996). As a consequence, it is probable that the role of the MWSA simulated by the ZC model is overestimated in comparison with the real world, Nevertheless, results of our comparisons suggest that the positive feedback mechanism associated with the meridional wind to some degree may be at work in reality, and may affect the mean stability of the system,

An important lesson of this study is that the anomaly structures associated with particular processes can be as important to the coupled variability as the anomaly amplitude. Some structures are configured much more favorably for strong coupled feedback than others. In this case, the SST anomaly patterns associated with MWSA forcing, though much weaker

in absolute terms than those associated with ZWSA, are very favorable for positive coupled feedback, and therefore play an important role in the coupled variability. In this and most likely in other models, seemingly small but systematic errors that arise in uncoupled component models can result, if configured unfavorably, in very large errors in coupled mode, In general, attention to structure as well as amplitude of errors is necessary.

dditional modeling and observational studies are needed to confirm the pi esent findings. One source of difficulty is the lack of observations. Considerable progress in observing the baroclinic currents has been made thanks to satellite altimetry, but the Ekman shear is not measurable from altimetry. In the future, one may benefit from interferometric radar imagery (Ainsworth et al, 1995) or drifter data (Frankignoul et al, 1996) to measure the surface velocities of the ocean. Using such observations, it will be particular y helpful to determine directly the contribution of the meridional Ekman currents to sea surface temperature variability in the equatorial eastern and central Pacific.

Acknowledgements

The authors at the Jet Propulsion Laboratory, California Institute of Technology were supported under contract with the National Aeronautics and Space Administration, S2 was supported through NSF grant ATM92-24915.

List of references

Ainsworth, T, L., S. R. Chubb, R. A, Fusina, R, M. Goldstein, R, W. Jansen, J.-S, Lee, and G. R. Valenzuela, 1995: INSAR Imagery of surface currents, wave fields, and fronts, IEEE Trans. on Geoscience and Remote Sensing, Special issue on surface and atmospheric remote sensing, 33, 1117-1123,

Barnett, T, P., M. Latif, E. Kirk and E. Roeckner, 1991: On ENSO physics, *J. Clim., 4,487-515.*

Battisti, D. S., 1988: Dynamics and thermodynamics of a warming event in a coupled tropical atmosphere-ocean model, *J. Atmos. Sci., 45,2889-2919.*

Battisti, D. S. and A, C. Hirst, 1989: Interannual variability in a tropical atmosphere-ocean model: influence of the basic state, ocean geometry and nonlinearit y. *J. Atmos. Sci., 46,* 1687-1712.

Bjerknes, J., 1969: Atmospheric teleconnections from the equatorial Pacific. *Mon. Wea. Rev.,* 97, 163-172.

Boulanger, J.-P, and C. Menkes, 1995: Propagation and reflection of long equatorial waves in the Pacific ocean during the 1992-1993 El Niño event, *J. Geophys. Res.,* **100,** 25041-25059.

Busalacchi, A., and J. J. O'Brien, 1981: Interannual variability of the equatorial Pacific in the 1960's. *J. Geophys. Res.,* 86, 10901-10907.

Cane, M, A., M. Munnich and S. E, Zebiak, 1990: A study of self-excited oscillation of the tropical Ocean Atmosphere system. Part 1: linear analysis, *J. Atmos. Sci.,* 47, 1562-1577.

Cane, M, A. and E. S. Sarachick, 1976: Forced baroclinic ocean motions, I: the linear equatorial unbounded case., *J Mar. Res., 34,629-665.*

Cane, M. A., and S. E. Zebiak, 1985: A theory for El Niño and the Southern Oscillation, *Science, 228, 1085-1087.*

Cane, M. A., S. E. Zebiak, and S. C. DoIan, 1986: Experimental forecasts of El Niño, *Nature, 321, 827-832.*

Delcroix, T., J-P, Boulanger, F. Masia and C, Menkes, 1994: GEOSAT-derived sea level and surface-current anomalies in the equatorial Pacific, during the 1986-1989 El Niño and La Niña. *J. Geophys. Res.,* 99, 25093-25107.

Frankignoul C., F. Bonjean and G. Reverdin, 1996: Interannual variability of surface currents in the tropical Pacific during 1987-1993, *J. Geophys. Res.,* in press.

Graham, N. E., and W, B. White, 1988: The El Niño cycle: a natural oscillator of the Pacific ocean-atmosphere, *Science, 240* 1293-1302.

Hayes, S. P., M. J. McPhaden and J. M. Wallace, 1989: The influence of sea surface temperature upon surface wind in the eastern equatorial Pacific. Weekly to monthly variability, *J. Clim.*, 2, 1500-1506.

Hirst, A. C., 1985: Free equatorial instabilities in simpled coupled atmosphere-ocean models, in *Coupled Ocean-Atmosphere models,* edited by J. C. J. Nihoul, 153-165, Elsevier, New-York.

Jin, F. F., and J, D. Neelin, 1993: Modes of interannual tropical ocean-atmosphere interaction-A unified view. Part I: Numerical results. *J. Atmos. Sci., 50, (21) 3477-3503.*

Kessler, W. S. and M. J, McPhaden, 1995: Equatorial waves and the dynamics of the 1991-1993 El Niño, *J. Clim., 8, 1757-1774.*

Kleeman, R., A, M, Moore and N. R, Smith, 1995: Assimilation of sub-surface thermal data into an intermediate tropical coupled ocean-atmosphere model, *Mon. Wea. Rev.,* **123,** in press.

Knox, R. A., and D. Halpern, 1982: Long range Kelvin wave propagation of transport variations in Pacific equatorial currents, *J. Mar, Res.*, 40, Suppl., 329-339,

Lau, K. M., 1981: Oscillations in a simple equatorial climate system, *J. Atmos. Sci., 38,248-261,*

McCreary ,J. P., and D. L. T. Anderson, 1984: A simple model of El Niño and the Southern Oscillation, Mon. *Wea. Rev., 112,934-946.*

Miller, L., R. E. Cheney, and B. Douglas, 1988: Geosat altimeter observations of Kelvin waves and the 1986-1987 El Niño, *Science, 239, 52-54.*

Moore, D. W., and S, G. H. Philander, 1977: Modeling of the tropical ocean circulation. (Chap, 8), *The* sea, Vol. 6, E. D. Goldberg, I. N. Cave, J. J. O'Brien and J. H. Steek, Eds., Interscience, 1048 pp.

Neelin, J. D., 1990: A hybrid coupled general circulation model for El Niño studies. *J. Atmos. Se.,* 47., 674-693.

Périgaud, C., and B. Dewitte, 1996: El Niño-La Niña events simulated with Cane and Zebiak's model and observed with satellite and in situ data. Part 1: model data comparison., *J. Clim., 9, 66-84.*

Philander, S. G. H. and W. J. Hurlin, 1988: The heat budget of the tropical Pacific ocean in a simulation of the 1982-83 El Niño, *J. Phys. Oceanog., 18,926-931.*

Philander, S. G. H. and A, D. Seigel, 1985: Simulation of El Niño 1982-83. *Coupled Ocean-Atmosphere Models,* J. C. Nihoul, Ed., Elsevier, 517-541.

Schopf P. S. and M. J. Suarez, 1988: Vacillations in a coupled ocean-atmosphere system, *J. Atmos. Sci. , 45, 3283-3287.*

Xie, S. P., 1994: "The maintenance of an equatorially asymmetric State in a Hybrid Coupled GCM", *J, Atmos. Sci.*, Vol. **51, 2602-2611,**

Yamagata, T., 1985: Stability of a simple air-sea coupled model in the tropics, in *Coupled Ocean-atmosphere models,* edited by J. C. J Nihoul, 637-658, Elsevier, New-York.

Zebiak, S. E., 1986: "Atmospheric Convergence feedback in a simple model for El Niño", *Month. Wea. Rev.,* **114**, 1263-1271.

Zebiak, S. E., 1990: Diagnostic studies of Pacific Surface winds, *J. Clim., 3, 1016-1031.*

Zebiak, S, E., and M, A. Cane, 1987: A model El Niño-Southern Oscillation. *Mon. Wea. Rev., 115,2262-2278.*

Figure Caption

Figure 1: Simulated Niño3 index as a function of time from coupled experiments with various initial conditions, Plain thick lines represent run CPD.TY0 and dashed lines represent run CPD.STD for the initial conditions of January 1980 **(a),** January 1983 **(b),** or for an initial kick with a pseudo-random wind patch (c).

Figure 2: Simulated Niño3 index as a function of time in coupled test experiments. **(a)** Experiments CPD.TYEk (heavy solid line) where TY has been put to zero in the shear calculation only and CPD.TYb (dashed line) where TY has been put to zero in the baroclinic dynamics calculation only. The thin solid line is the standard run CPD.STD. **(b)** Experiments CPD.TYEkfilteq (heavy solid line) where TY has been filtered out specifically in the equatorial band and CPD.TYEkfiltoff (dashed line) where TY has been filtered out specifically outside the equatorial band, The thin solid line is for the run CPD.STD.

Figure 3: Change of temperature (in "C per month) due to each of the eight terms involved in the SST equation (averaged over Niño3 region) as a function of time. The numbering of the curves corresponds to the numbering of the terms of the SST equation as described in the text.

Figure 4: Warm event anomalous vertical current and induced temperature change simulated in the standard run, **(a)** Total vertical current anomaly field (due to baroclinic and Ekman currents induced by the zonal and meridional) winds, with shaded regions corresponding to downwelling. Equatorial

sections (2°S-20N) of the vertical current anomaly due to the Ekman currents driven by the zonal only **(b)** or meridional only (c) wind stress anomalies (thin solid lines). The dashed lines represent the total anomalous vertical current, the thick solid lines represent the term proportional to the ZWSA in Fig.4b and the one proportional to the meridional gradient of the MWSA in Fig 4c. Equatorial section of temperature changes **(d)** induced by the ZWSA (dashed line) and by the MWSA (solid line), Units of current anomaly and temperature change are 10^{-3} cms-^{1} and °Cmonth^{-1}.

Figure 5: Experiments where the ocean model is forced by FSU wind stress anomalies over 1980-1995, with both wind components (CR.STD) or with the zonal component only (CR. TY0). **(a)** Niño3 index as a function of time. Plots are for run CR.TY0 (plain), CR.STD (dashed). SST maps simulated on January 1983 by CR.STD **(b),** CR.TY0 (c) and their difference **(d).** Shaded regions correspond to cold anomalies.

Figure 6: Amplitude maps of the first EOF for the observed ZWSA **(a)** and MWSA **(b)** or for the simulated ZWSA (c) and MWSA **(d).** Values are normalized (see text) and one unit corresponds to ?? Pa m^{-1}. Shaded regions correspond to negative anomalies (easterlies and northerlies).

Figure 7: Vertical current anomaly simulated in the standard run. **(a)** anomaly field (due to the Ekman currents induced by the zonal and meridional) observed winds, with shaded regions corresponding to downwelling. Equatorial sections (2°S-2°N) of the vertical current anomaly due to the Ekman current driven by the zonal only **(b)** or meridional only (c) wind stress anomaly for observation (solid lines) or model (dashed lines).

(d) Temperature change induced by the ZWSA (dashed line) and by the MWSA (solid line), with the thick lines for observations and the thin lines for model. Units of currents and temperature changes are 10^{-3} cm s^{-1} and ^{o}Cmonth^{-1}.

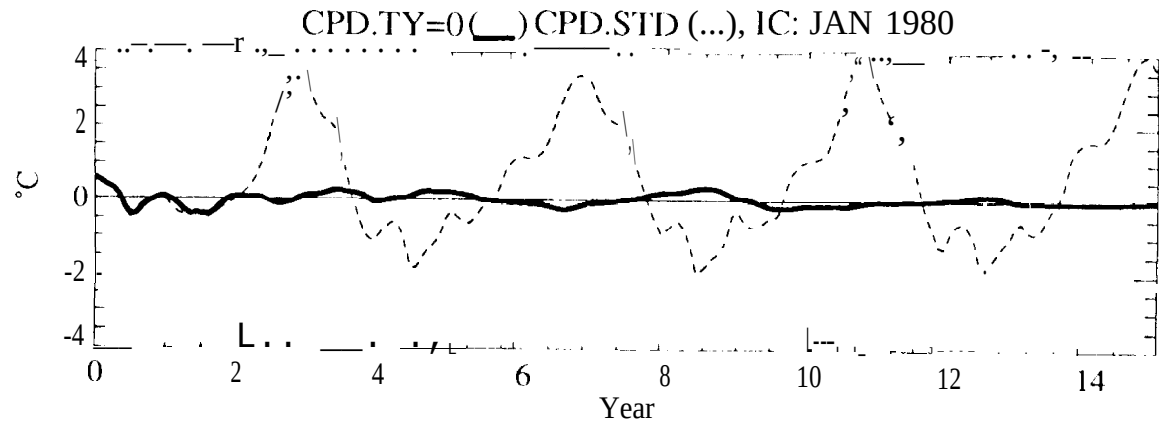
CPD.TY=0 (__) CPD.STD (...), IC: JAN 1980
°C
4
2
0
-2
-4
0
2
4
6
8
10
12
14
Year

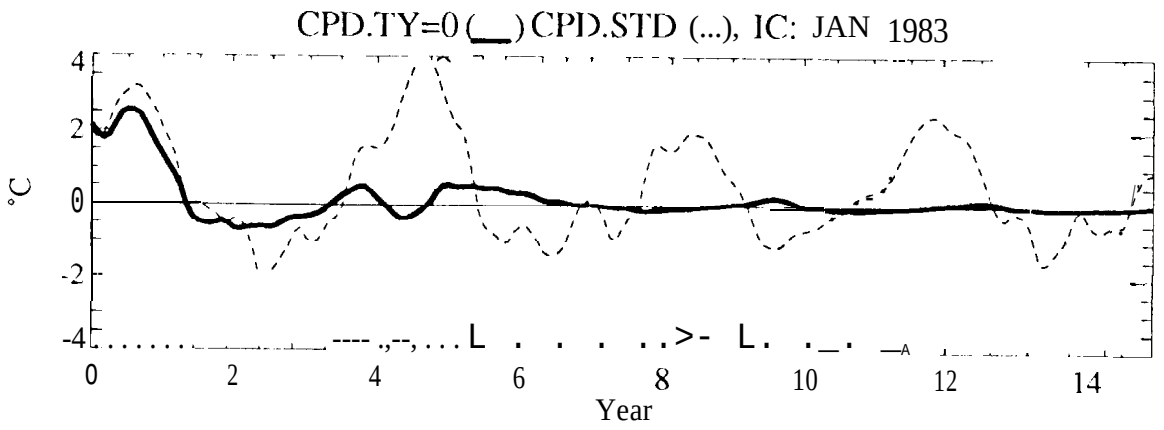
CPD.TY=0 (__) CPD.STD (...), IC: JAN 1983
°C
4
2
0
-2
-4
0
2
4
6
8
10
12
14
Year

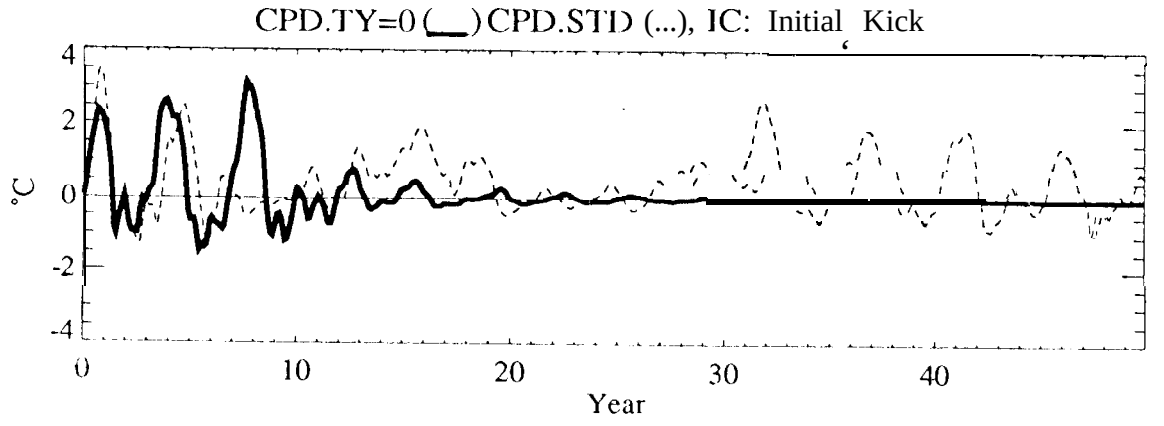
CPD.TY=0 (__) CPD.STD (...), IC: Initial Kick
°C
4
2
0
-2
-4
0
10
20
30
40
Year

figure 1

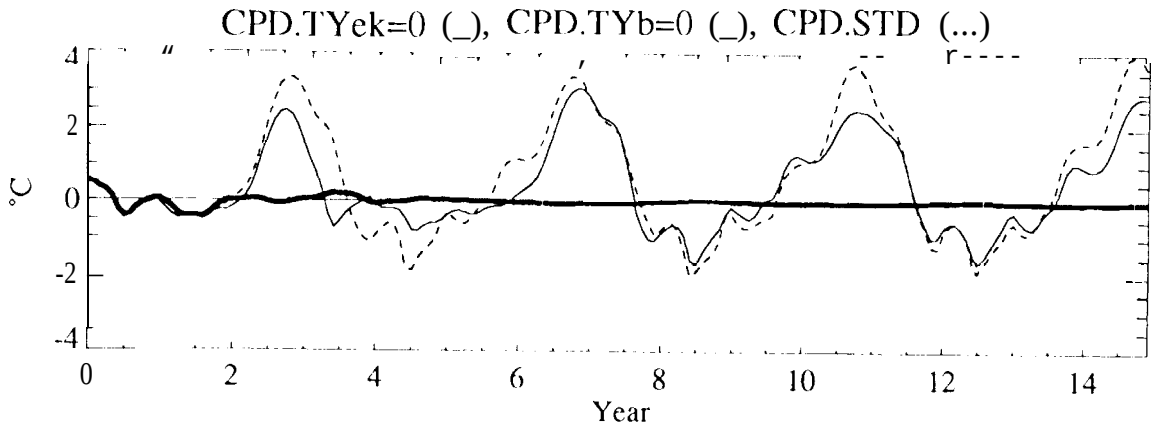
CPD.TYek=0 (_), CPD.TYb=0 (_), CPD.STD (...)
°C
4
2
0
-2
-4
0
2
4
6
8
10
12
14
Year

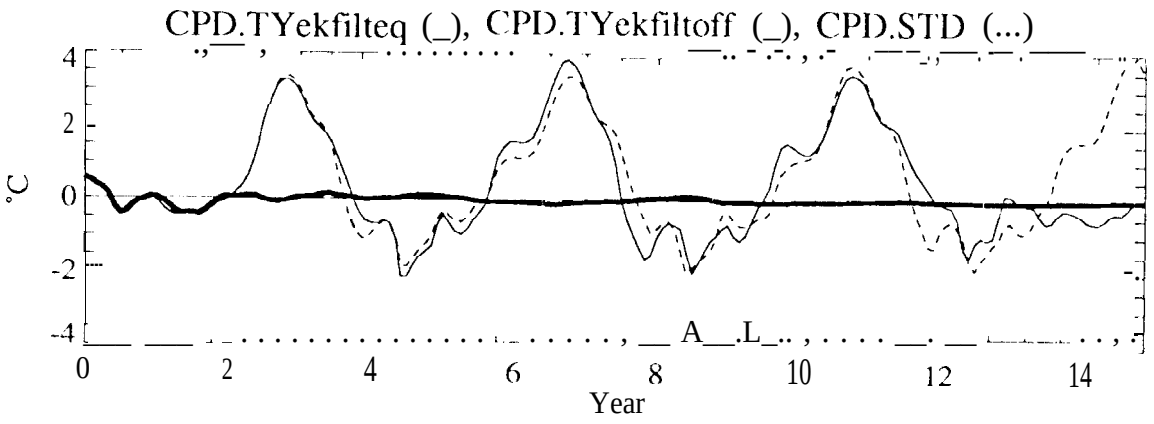
CPD.TYekfilteq (_), CPD.TYekfiltoff (_), CPD.STD (...)
°C
4
2
0
-2
-4
0
2
4
6
8
10
12
14
Year

Figure 2

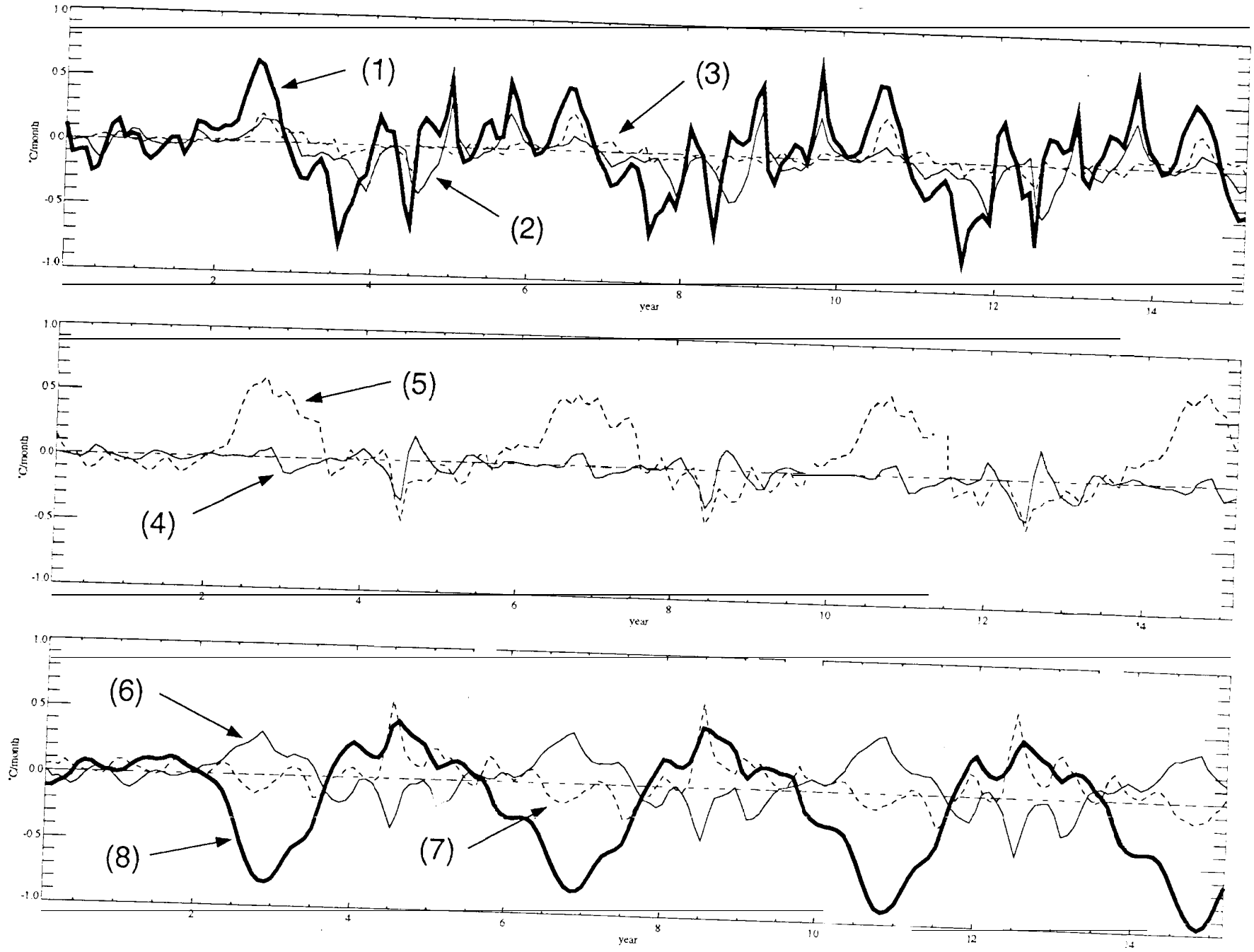

Figure 3

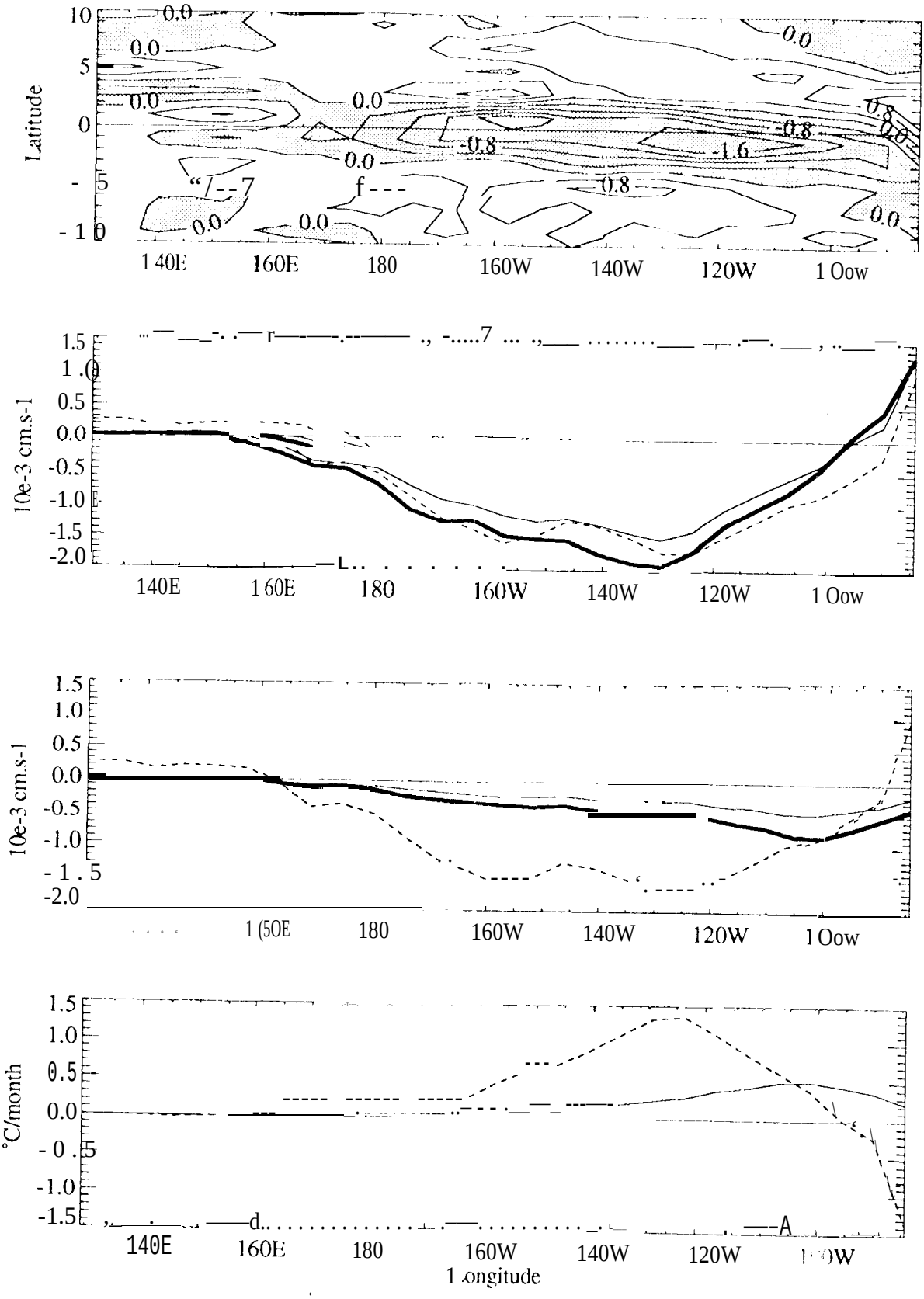
Latitude
10
5
0
- 5
- 10
0.0
0.8
1.6
140E
160E
180
160W
140W
120W
1 Oow
10e-3 cm.s-1
1.5
1.0
0.5
0.0
-0.5
-1.0
-1.5
-2.0
°C/month
Longitude

Figure 4

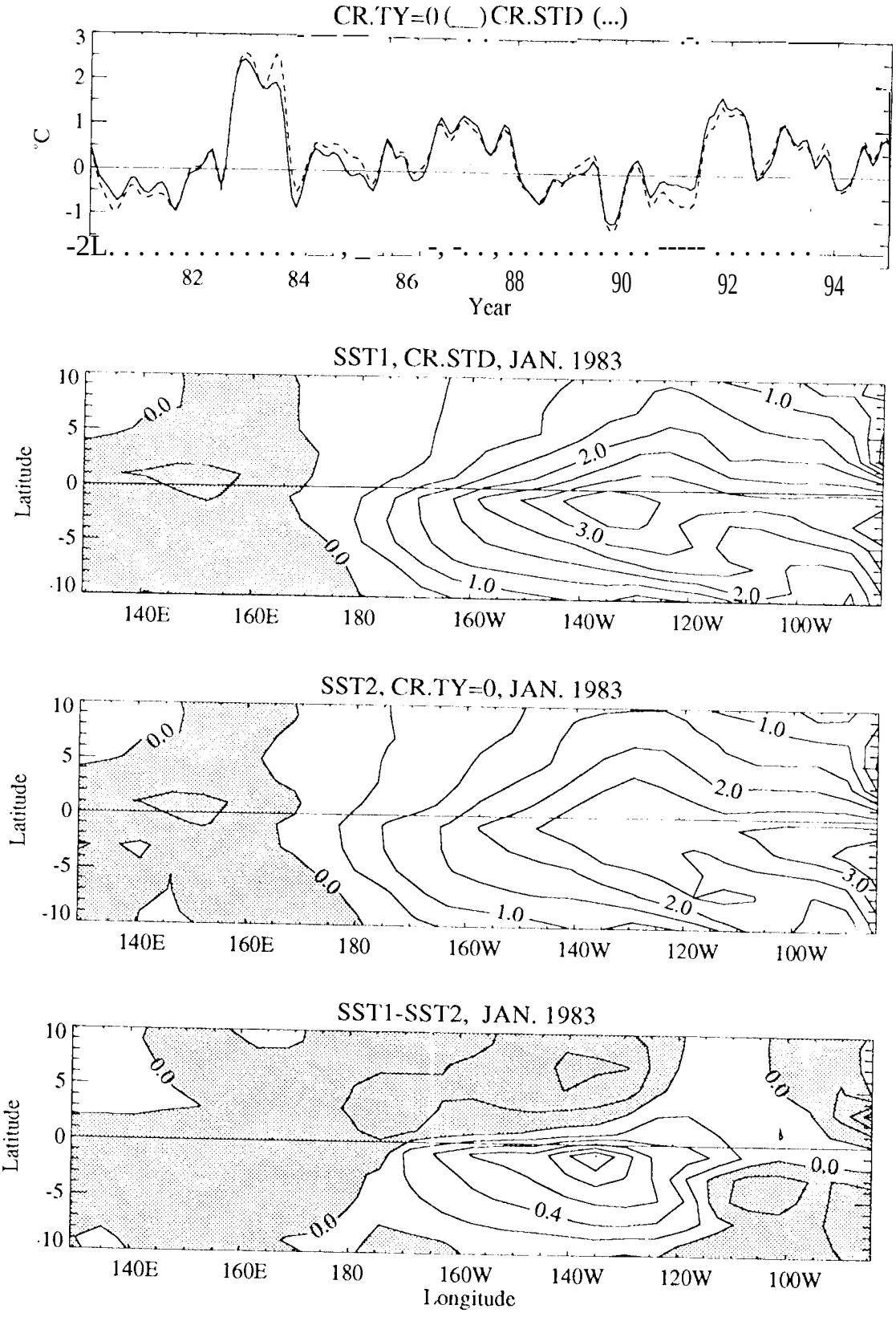
CR.TY=0 (__) CR.STD (...)
°C
Year
SST1, CR.STD, JAN. 1983
SST2, CR.TY=0, JAN. 1983
SST1-SST2, JAN. 1983
Latitude
Longitude
140E
160E
180
160W
140W
120W
100W

Figure 5

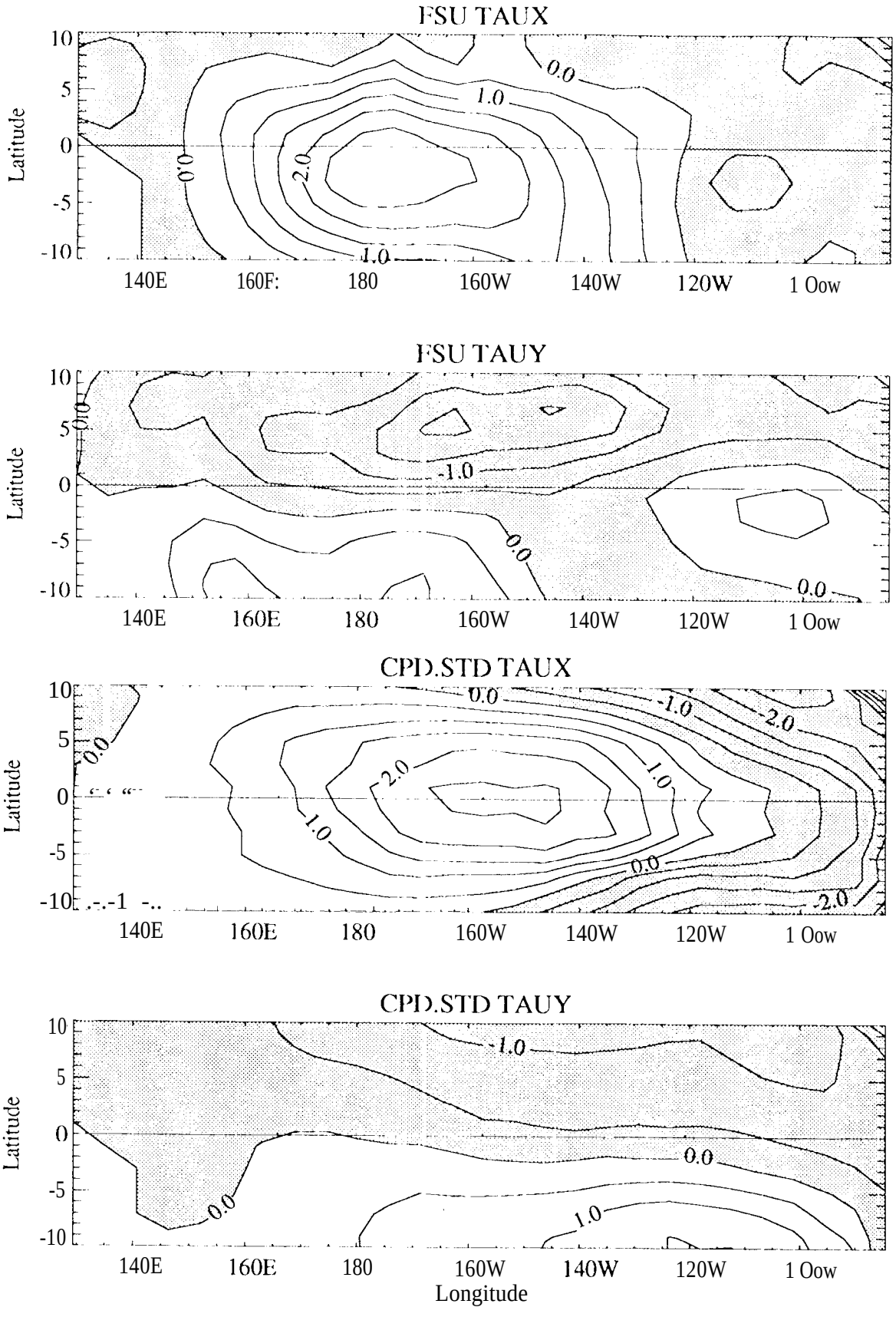
FSU TAUX
Latitude
10
5
0
-5
-10
0.0
1.0
2.0
-1.0
140E
160F:
180
160W
140W
120W
1 Oow
FSU TAUY
Latitude
10
5
0
-5
-10
0.0
-1.0
0.0
0.0
140E
160E
180
160W
140W
120W
1 Oow
CPD.STD TAUX
Latitude
10
5
0
-5
-10
0.0
-1.0
-2.0
0.0
2.0
1.0
-1.0
0.0
-2.0
140E
160E
180
160W
140W
120W
1 Oow
CPD.STD TAUY
Latitude
10
5
0
-5
-10
-1.0
0.0
0.0
1.0
140E
160E
180
160W
140W
120W
1 Oow
Longitude

Figure 6

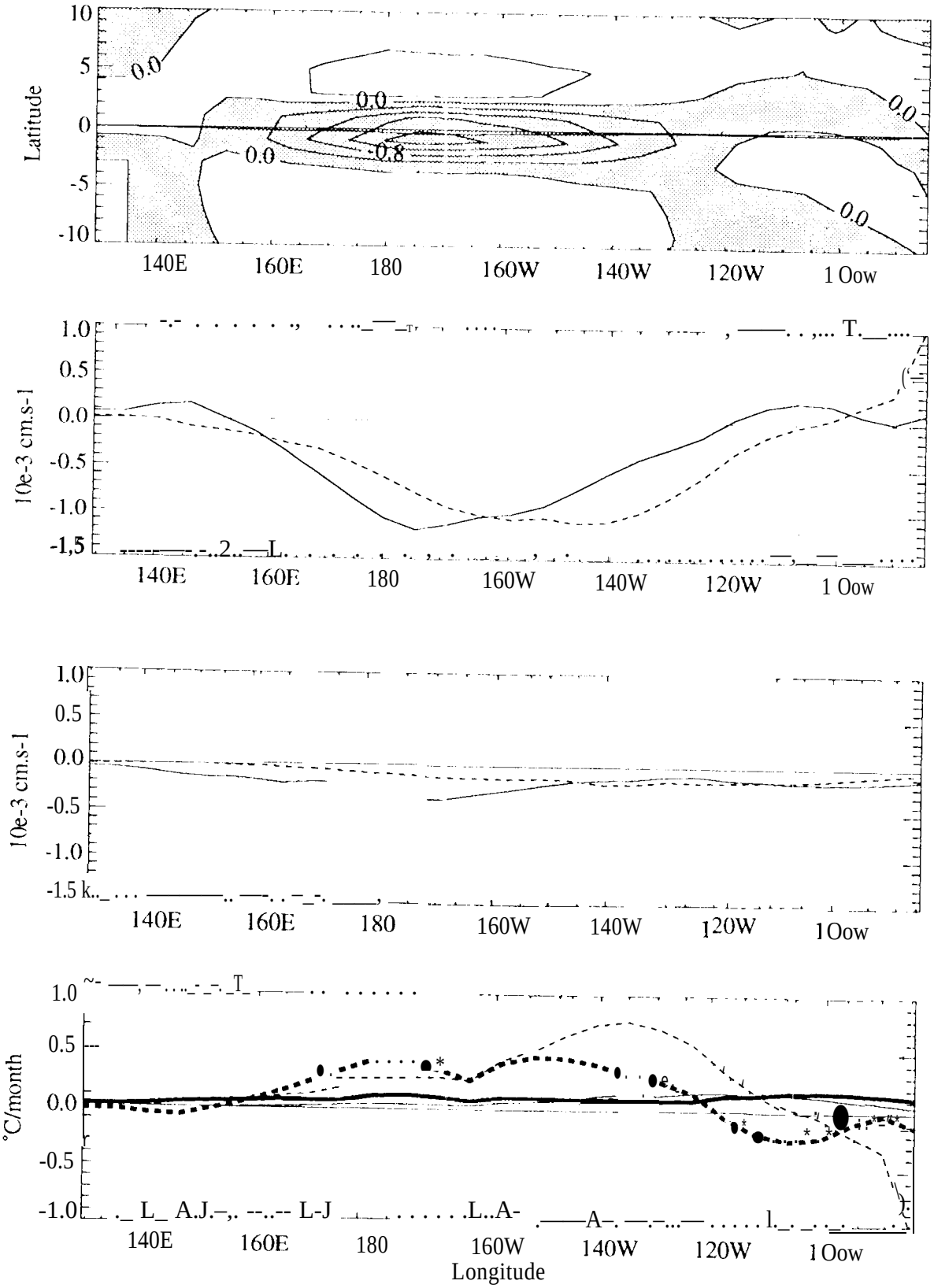
10
5
0
-5
-10
Latitude
0.0
0.0
0.0
-0.8
0.0
0.0
140E
160E
180
160W
140W
120W
1 Oow
1.0
0.5
0.0
-0.5
-1.0
-1,5
10e-3 cm.s-1
140E
160E
180
160W
140W
120W
1 Oow
1.0
0.5
0.0
-0.5
-1.0
-1.5 k..
10e-3 cm.s-1
140E
160E
180
160W
140W
120W
1Oow
1.0
0.5
0.0
-0.5
-1.0
°C/month
140E
160E
180
160W
140W
120W
1Oow
Longitude

Figure 7